BIOCHEMISTRY
including biophysical chemistry & molecular biology

Article

pubs.acs.org/biochemistry

Lipid-Directed Vinculin Dimerization

Krishna Chinthalapudi,[†,‡] Dipak N. Patil,[†,‡] Erumbi S. Rangarajan,[†,‡] Christoph Rader,[‡,§] and Tina Izard*[,†,‡]

[†]Cell Adhesion Laboratory, [‡]Department of Cancer Biology, and [§]Department of Molecular Therapeutics, The Scripps Research Institute, Jupiter, Florida 33458, United States

ABSTRACT: Vinculin localizes to cellular adhesions where it regulates motility, migration, development, wound healing, and response to force. Importantly, vinculin loss results in cancer phenotypes, cardiovascular disease, and embryonic lethality. At the plasma cell membrane, the most abundant phosphoinositide, phosphatidylinositol 4,5-bisphosphate (PIP_2), binds the vinculin tail domain, Vt, and triggers homotypic and heterotypic interactions that amplify binding of vinculin to the actin network. Binding of PIP_2 to Vt is necessary for maintaining optimal focal adhesions, for organizing stress fibers, for cell migration and spreading, and for the control of vinculin dynamics and turnover of focal adhesions. While the recently determined Vt/PIP_2 crystal structure revealed the conformational changes occurring upon lipid binding and oligomerization, characterization of PIP_2-induced vinculin oligomerization has been challenging in the adhesion biology field. Here, via a series of novel biochemical assays not performed in previous studies that relied on chemical cross-linking, we characterize the PIP_2-induced vinculin oligomerization. Our results show that Vt/PIP_2 forms a tight dimer with Vt or with the muscle-specific vinculin isoform, metavinculin, at sites of adhesion at the cell membrane. Insight into how PIP_2 regulates clustering and into mechanisms that regulate cell adhesion allows the development for a more definite sensor for PIP_2, and our developed techniques can be applied generally and thus open the door for the characterization of many other protein/PIP_2 complexes under physiological conditions.

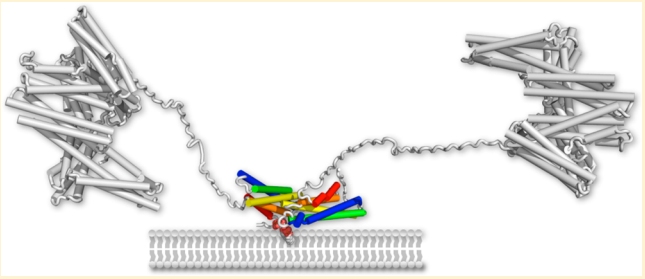

Actin stress fibers and networks attach to the plasma membrane via a number of cytoskeletal proteins such as vinculin to consolidate linkages between the membrane and the cytoskeleton and to increase the strength of adhesion to substrates. Like vinculin, most of these proteins are activated first to allow them to bind to actin, and interfering with phosphoinositide binding disrupts linking of the membrane to the cytoskeleton. Vinculin is one of several actin cross-linking and membrane attachment proteins that are regulated by PIP_2. Once activated, vinculin binds PIP_2, which is necessary for maintaining optimal focal adhesions, for organizing the actin cytoskeleton, and for cell migration and spreading.[1] The alternatively spliced vinculin isoform termed metavinculin heterodimerizes with vinculin and plays essential roles in muscle and cardiac cells.

Vinculin is a highly conserved cytoskeletal scaffolding protein that localizes to adherens junctions and focal adhesions[2] and plays crucial roles in regulating the cellular responses to tension by linking the transmembrane integrin and cadherin receptors to the actin cytoskeleton. Vinculin also regulates focal adhesion formation and cell migration.[3] Significantly, vinculin knockout mice die by day E10.5,[4] and fibroblasts from these mice are defective in adhering, spreading, and migrating; exhibit increased levels of FAK and paxillin signaling and reduced cell stiffness; and are resistant to apoptosis and anoikis.[5−11] Vinculin is kept in a closed, inactive conformation via extensive hydrophobic interactions between its helical 91 kDa vinculin head domain (VH) and its 21 kDa five-helix bundle vinculin tail domain (Vt).[12−15] Several binding partners have been identified to bind to activated vinculin in its open conformation. For example, talin,[13,16−19] α-actinin,[20,21] α-catenin,[22−25] β-catenin,[26] and E-cadherin[2,27] bind to VH. The vasodilator-stimulated phosphoprotein,[28] ponsin/CAP,[29] vinexin α and β,[30] and the Arp2/3 complex[31] bind to the proline-rich region, while paxillin,[32] raver1,[33−36] filamentous actin (F-actin),[37] and phosphatidylinositol 4,5-bisphosphate (PIP_2)[38] bind to Vt. Binding to Vt is specific for acidic phospholipids such as phosphatidylserine (PS), phosphatidylinositol (PI), and PIP_2.[38−42]

A muscle-specific splice variant of vinculin, termed metavinculin, is co-expressed with vinculin,[43] and both isoforms localize to the cell membrane, the I-band in the sarcomere, and intercalated discs.[44] Vinculin is a 1066-residue protein, and metavinculin has a 68-residue insert after vinculin residue 915, which alters its functions[45] such as having a higher affinity for raver1[33,34] and a lower affinity for PIP_2[46] compared to those of Vt, resulting in a 1134-residue ~150 kDa protein.[7] Their identical head domains bind to several membrane-associated proteins mentioned above, whereas their distinct tail domains have unique actin organization functions.[47]

Received: January 6, 2015
Revised: April 8, 2015
Published: April 16, 2015

DOI: 10.1021/acs.biochem.5b00015
Biochemistry 2015, 54, 2758−2768

Metavinculin expression, which is always co-expressed with vinculin, differs in muscle tissues, and the level of expression is highest in smooth muscle.[44,45,48,49] There are also functional differences in the two vinculin tail isoforms; for example, MVt and Vt bundle F-actin differently,[47,50] and MVt binds raver1 more tightly than Vt.[33,35] Moreover, binding of metavinculin to phospholipids is impaired compared to binding of vinculin, and metavinculin does not form oligomers even in the presence of PIP_2. However, metavinculin does form a heterodimer with PIP_2-bound vinculin.[46,50]

Interestingly, Vt oligomerizes under certain conditions and with certain binding partners and even dimerizes at high concentrations in the absence of ligands.[14,51] At physiological concentrations, Vt homodimerizes in the presence of actin[14,37,52] and oligomerizes in the presence of PIP_2.[14,42,53] Our recently determined Vt/PIP_2 crystal structure (Protein Data Bank entry 4pr9) showed that one PIP_2 molecule is sandwiched between three Vt molecules, two of them engaging in a swapped domain-like arrangement of their C-terminal coiled coil regions. Further, PIP_2 binding releases the N-terminal coiled coil region, and the structure-guided K944Q/R945Q or K1061Q mutants failed to bind to PIP_2 vesicles.[1]

The first evidence of vinculin oligomerization was provided using rotary-shadowed EM[54,55] showing tetramers and higher-order oligomers that formed head−head and tail−tail interactions.[56] Vt self-associates to form a dimer with a binding constant of ∼0.3 mM[51] as seen in the Vt crystal structure[14] and in solution by nuclear magnetic resonance,[42,51] cryo-EM,[52] or electron paramagnetic resonance.[57] Furthermore, Vt forms multiple high-molecular weight bands upon cross-linking, suggesting that different oligomers may form.[53,58,59] However, the self-association of Vt seems to be physiologically irrelevant according to its weak K_d.[60] PIP_2 also induces Vt oligomers,[46,53] and PIP_2 has been suggested to play other roles, including facilitating PKC phosphorylation,[61] preventing F-actin binding,[62] promoting membrane associations,[63] and regulating focal adhesion turnover.[64] More recently, binding to PIP_2 has been shown to be necessary for maintaining optimal focal adhesions, for organizing stress fibers, and for cell migration and spreading.[1]

Because the binding of MVt to acidic phospholipids is weaker than that of Vt, PIP_2-directed dimerization is less likely for MVt.[46] However, MVt readily heterodimerizes with PIP_2-adsorbed Vt.[46,50] Functional studies of the PIP_2-directed vinculin dimer have been challenging because of the technical difficulties associated with lipid-binding proteins. Our recently developed lipid-binding deficient Vt mutants now finally allow the study of the important roles and mechanisms of PIP_2 in the regulation of vinculin at focal adhesions[1] and perhaps adherens junctions. Because all biochemical studies of the PIP_2-directed vinculin dimer relied on chemical cross-linking and/or the use of what later turned out to be unstable Vt truncations,[3,42,64−68] the oligomerization of vinculin in cells has not been observed. Our novel assays for assessing the oligomeric state of vinculin that do not suffer from artifacts that plagued previous studies can be applied to many other adhesion proteins.

MATERIALS AND METHODS

DNA Constructs, Protein Expression, and Purification. Human metavinculin tail domain (MVt) constructs (residues 879−1134, 945−1134, and 959−1130) were cloned into the modified pET28 vector using *Nde*I and *Bam*HI restriction sites to create an N-terminal His_8 tag that can be cleaved by PreScission protease. The cloning of a human vinculin tail (Vt) domain construct (residues 879−1066) has already been reported.[17] After sequence verification, the clones were transformed into BL21(DE3) cells for expression in auto-induction medium.[69] Purification of these proteins was conducted as described previously.[50]

Vt, MVt, and Vt mutant (R1060A, K915Q/K944Q/R945Q, K915Q/K1061Q, and K944Q/R945Q/K1061Q) proteins were purified as described previously.[1] Human merlin FERM (residues 1−339) was amplified and cloned into the pGEX-6P-1 expression vector (GE Life Sciences). The full-length human merlin A585W/R588K mutant was generated from a human merlin construct (addgene plasmid number 11629) using Agilent Technology's QuickChange site-directed mutagenesis kit. Mutations were confirmed by sequencing. Proteins were expressed in *Escherichia coli* strain BL21(DE3) RIL (Stratagene) at 18 °C for 20 h in Luria-Bertani medium with ampicillin using 0.1 mM isopropyl β-D-1-thiogalactopyranoside (IPTG). Cells were harvested by centrifugation at 5000*g* for 10 min and lysed in buffer A [20 mM HEPES (pH 7.5), 400 mM NaCl, and 0.1 mM EDTA]. Cells were disrupted using a French press; the lysate was centrifuged at 30000*g* for 45 min, and the supernatant was applied to a GST column equilibrated with buffer A. The proteins were eluted with 10 mM glutathione in buffer A. The GST fusion proteins were dialyzed into 20 mM HEPES (pH 7.5), 400 mM NaCl, 1 mM DTT, and 0.1 mM EDTA and digested with PreScission protease at 4 °C. The proteins were further purified by gel filtration using a 26/60 Superdex 200 column (GE Healthcare) that was pre-equilibrated with 20 mM HEPES (pH 7.5), 400 mM NaCl, 1 mM DTT, and 0.1 mM EDTA.

DNA of chicken vinculin tail domains (residues 884−1066) fused to either CFP (addgene plasmid number 46180) or YFP (addgene plasmid number 46181) at its N-terminus in pET-15b expression vectors was obtained from addgene. The K1061Q mutation was introduced into both CFP-Vt and YFP-Vt constructs by using the site-directed mutagenesis kit (Agilent Technologies). DNA sequences were verified for all constructs.

BL21-CodonPlus (DE3)-RIL cells (Stratagene) were transformed with pET15b vectors encoding CFP-Vt, YFP-Vt, CFP-Vt K1061Q, or YFP-Vt K1061Q. For expression, 3 L of LB medium was inoculated, and the expression of polyhistidine-tagged recombinant proteins was induced at an OD of 0.6−0.7 using 1 mM IPTG at 37 °C. After being induced for 4 h, cells were collected by centrifugation at 5000 rpm for 20 min. Cell pellets were resuspended in a buffer containing 50 mM Tris (pH 7.5), 400 mM NaCl, 1 mM PMSF, and 1 mM benzamidine. Cells were lysed using a sonicator, and the clarified supernatant was obtained by centrifugation at 35000 rpm for 30 min. Recombinant proteins were first purified by a Ni^{2+}-NTA affinity column followed by gel filtration using a Superdex 75 10/300 GL column on an FPLC purification system (GE Healthcare, ÄKTA purifier).

In Vitro Chemical Cross-Linking. *In vitro* chemical cross-linking of Vt (residues 891−1066), lipid-binding deficient Vt mutants (K1061Q, K915Q/K944Q/R945Q, K915Q/K1061Q, and K944Q/R945Q/K1061Q), full-length human merlin, and the merlin N-terminal domain was conducted in triplicate as described previously[46,53] with some modification. Briefly, purified proteins were incubated with and without PIP_2, PC micelles, or PC/PIP_2 micelles (15% PIP_2) at 37 °C for 30 min followed by incubation with a chemical cross-linker at 30 °C for

DOI: 10.1021/acs.biochem.5b00015
Biochemistry 2015, 54, 2758−2768

30 min in NaH_2PO_4 (pH 7.2), 7 mg/mL *N*-hydroxysulfosuccinimide (NHS) (Sigma-Aldrich), and 1.5 mg/mL 1-ethyl-3-[3-(dimethylamino)propyl]carbodiimide (EDC) (Sigma-Aldrich). The reactions were terminated by addition of SDS−PAGE sample buffer [250 mM Tris-HCl (pH 6.8), 10% SDS, 30% glycerol, 0.5 M DTT, and 0.25% bromophenol blue] and boiling, and cross-linking was analyzed by SDS−PAGE.

Vt and MVt Heterodimer Interaction. Varying concentrations (0−15 μM) of Vt (residues 879−1066) were incubated with different concentrations (0−12 μM) of MVt (residues 859−1134) in the presence of a 10-fold excess of PIP_2 at 37 °C for 30 min. The samples were then resolved on a 10−15% PHAST gel using SDS buffer strips and visualized by Coomassie blue staining.

Size Exclusion Chromatography. Vt (residues 891−1066), MVt (residues 959−1130), and Vt/MVt in the absence or presence of a PIP_2 derivative having a short phosphoinositide chain [$(CH_2)_8$] were run on a Superdex 200 10/300 GL (GE Healthcare, model no. 17-5175-01) chromatography column equilibrated with 20 mM Tris buffer (pH 8), 400 mM NaCl, 0.1 mM EDTA, and 1 mM DTT at 4 °C. Vt and MVt (100 μM) were incubated with PIP_2 (100, 200, and 300 μM), and Vt and MVt (100 μM each) were incubated with PIP_2 (100 and 200 μM) on ice for 1 h. The protein/PIP_2 complexes were loaded onto a calibrated Superdex 200 column and eluted at a flow rate of 0.5 mL/min. Columns were additionally calibrated with the gel filtration calibration kit from GE life sciences.

Fluorescence Resonance Energy Transfer (FRET) Assay. Recombinant purified proteins were used for FRET measurements. The emission spectra of fluorescently tagged proteins were optimized for CFP-Vt at an excitation wavelength of 414 nm with a 455 nm cutoff filter and YFP-Vt at an excitation wavelength of 477 nm with a 495 nm cutoff filter and a bandwidth of 2 nm. The emission maxima at 475 nm were observed for CFP-Vt upon excitation at 414 nm, and the emission maxima at 528 nm were observed for YFP-Vt upon excitation at 475 nm. The concentrations that were used for optimizing the emission scan of CFP-Vt were 0.1, 0.5, 1.0, and 1.5 μM and for YFP-Vt were 1, 2, 3, and 4 μM.

PIP_2 micelles (80% PC, 20% PIP_2) were prepared as described previously.[1] For FRET measurements, 1.5 μM CFP-Vt/K1061Q and 4 μM YFP-Vt/K1061Q proteins were mixed and diluted with 20 mM Tris (pH 7.5) and 150 mM NaCl to a total volume of 100 μL. Next, freshly prepared PIP_2 micelles were added to the CFP- and YFP-labeled proteins in the concentration range of 0−500 μM and incubated for 10 min on ice. At higher concentrations (>300 μM PIP_2), the proteins tended to precipitate. The reaction mixtures were transferred into a 96-well plate (PerkinElmer), and the fluorescence emission spectrum of each well was measured with a Spectramax M5 fluorescence multiwell plate reader (Molecular Devices, Sunnyvale, CA). Data were collected from at least three different independent experiments for fluorescently labeled wild-type and K1061Q mutant Vt.

Immunochemistry. Western blot analyses for PIP_2-mediated oligomerization of Vt and various MVt constructs were conducted by incubating ∼8 μM protein with varying fold excess concentrations of PIP_2 (1-, 5-, 10-, and 20-fold) at 37 °C for 30 min and further subjected to chemical cross-linking with EDC/NHS as described. The samples were then resolved on a 10 to 15% gradient PHAST gel using SDS buffer strips and blotted onto an Immobilon-P membrane (Millipore) using a Bio-Rad semidry transfer apparatus. Subsequently, the blots were blocked with 5% nonfat dry milk, incubated with HRP-conjugated anti-His antibody, and developed with chemiluminescence substrate (Thermo Scientific) by following the suggested protocol.

Surface Plasmon Resonance. Binding studies of Vt (residues 879−1066) and MVt (residues 879−1134) were performed at 25 °C using a Biacore 2000 (Biacore AB, Uppsala, Sweden) equipped with a carboxymethyl dextran-coated gold surface (CM5 sensor chip, Biacore AB). The carboxymethyl groups on the chip were activated with 1-ethyl-3-[3-(dimethylamino)propyl]carbodiimide and *N*-hydroxysuccinimide to form the *N*-hydroxysuccinimide ester of carboxymethyl dextran. The interaction of Vt and MVt with PIP_2 was studied at 25 °C in a buffer containing 10 mM HEPES, 150 mM NaCl, 0.005% P-20, and 0.1 mg/mL BSA. Vt (approximately 6000 RU) and MVt were immobilized as well as reference flow cells that served for the subtraction of any background signal and nonspecific binding. PIP_2 was passed over all surfaces. Immobilization of Vt [in 10 mM sodium acetate (pH 5.0)] was performed using HBS-P buffer [10 mM HEPES (pH 7.4), 150 mM NaCl, and 0.005% P-20] at 25 °C using standard amine coupling chemistry.

Direct immobilization of MVt to the CM5 chip surface was not possible because of MVt precipitation in sodium acetate, and therefore, MVt was biotinylated and captured on the streptavidin surface, which was built on a reference and a reaction surface flow cell using standard amine coupling chemistry at a density of ∼9000 RU. MVt was incubated with NHS-biotin at an equimolar ratio in HBS-P buffer for 2 h. Free biotin was removed from the solution using a fast desalting column. Biotinylated MVt was captured on the streptavidin surface flow cell at an approximate density of 5000 RU. Data fitting was performed using BIAEvaluation 4.1 (Biacore AB). The binding dissociation constants were calculated from the observed on and off rates for the interactions.

RESULTS

Chemical Cross-Linking Results in Artifactual Vinculin Oligomerization. As it is the standard assay in the adhesion field, we used the established cross-linking assay to assess the oligomerization of vinculin upon binding to PIP_2. Recombinant Vt was incubated with various amounts of PIP_2 or PIP_2/PC or PC micelles and analyzed via SDS−PAGE in the presence or absence of [3-(dimethylamino)propyl]carbodiimide (EDC). As reported previously,[14,39,41,42,46,70] Vt oligomerizes only when it is bound to PIP_2 and PIP_2-containing micelles but not PC micelles (lanes d and e vs lane f in Figure 1A). Furthermore, Vt dimerizes in the absence of acidic phospholipids, which could be detected by SDS−PAGE only after chemical cross-linking with EDC (lane b in Figure 1A). In the presence of 30 μM PIP_2 and EDC, vinculin trimers and tetramers were observed (lane d in Figure 1A). Significantly, PC micelles containing 15% PIP_2 induced higher-order oligomers, and up to at least vinculin hexamers were readily visible via SDS−PAGE (lane e in Figure 1A).

We next tested the robustness of the established cross-linking assay on Vt mutants that are significantly impaired (>90% decrease) in their ability to cosediment with unilamellar vesicles containing 15% PIP_2.[1] In the presence of EDC, which generates zero-order cross-links between carboxylic acids and amino groups, all lipid-binding deficient mutants surprisingly formed oligomers as seen for the wild type and the R1060A Vt control

DOI: 10.1021/acs.biochem.5b00015
Biochemistry 2015, 54, 2758−2768

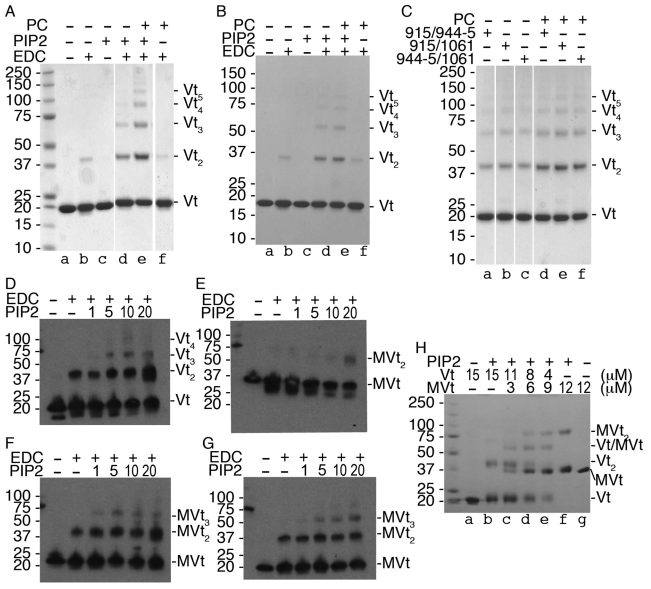

Figure 1. Binding of vinculin to PIP_2 induces the formation of oligomers. (A) SDS−PAGE of Vt (residues 891−1066) after EDC cross-linking to reveal oligomerization (Vt dimers, Vt_2; Vt trimers, Vt_3; etc.) as a consequence of 30 μM PIP_2 (lane d) or 5 μL of 15% PIP_2 in PC/PIP_2 micelles (lane e). PIP_2 oligomerization is specific as 5 μL of PC micelles (lane f) does not result in Vt oligomers (0% in the absence of PIP_2 vs up to 14% in the presence of PIP_2 in lanes d and e and only 7% dimer formation in the absence of PIP_2 vs up to 29% in the presence of PIP_2 in lanes d and e as judged by densitometry analyses). (B) SDS−PAGE of R1060A PIP_2-binding mutant Vt after EDC cross-linking to reveal oligomerization as a consequence of PIP_2 (30 μM, lane d) or 15% PIP_2 in PC/PIP_2 micelles (lane e). PIP_2 oligomerization is specific, as PC micelles (lane f) do not result in Vt oligomers (0% in the absence of PIP_2 vs up to 8% in the presence of PIP_2 in lanes d and e and only 7% dimer formation in the absence of PIP_2 vs up to 23% in the presence of PIP_2 in lanes d and e as judged by densitometry analyses). (C) SDS−PAGE of K915Q/K944Q/R945Q (lanes a and d), K915Q/K1061Q (lanes b and e), and K944Q/R945Q/K1061Q (lanes c and f) mutant Vt after EDC cross-linking (EDC/NHS is present in all lanes) to reveal oligomerization as a consequence of 30 μM PIP_2 (lanes a−c; 20, 6, and 3% for K915Q/K944Q/R945Q mutant Vt_2, Vt_3, and Vt_4, respectively; 19, 7, and 3% for K915Q/K1061Q mutant Vt_2, Vt_3, and Vt_4, respectively; 20, 6, and 2% for K944Q/R945Q/K1061Q mutant Vt_2, Vt_3, and Vt_4, respectively) or in 15% PIP_2 in 5 μL of PC/PIP_2 micelles (lanes d−f; 27, 11, 3, and 1% for K915Q/K944Q/R945Q mutant Vt_2, Vt_3, Vt_4, and Vt_5, respectively; 28, 11, 4, and 2% for K915Q/K1061Q mutant Vt_2, Vt_3, Vt_4, and Vt_5, respectively; 29, 10, 3, and 2% for K944Q/R945Q/K1061Q mutant Vt_2, Vt_3, Vt_4, and Vt_5, respectively, as judged by densitometry analyses). All lanes contain PIP_2 (30 μM in lanes a−c and 15% in lanes d−f). (D−G) Anti-His immunoblot blot of (D) Vt (residues 879−1066), (E) MVt (residues 879−1134), (F) MVt (residues 945−1134), and (G) MVt (residues 959−1130) in the presence of PIP_2 after EDC cross-linking to reveal oligomerization (Vt dimers, Vt_2; Vt trimers, Vt_3; etc.; or MVt dimers, MVt_2; MVt trimers, MVt_3; etc.) as a consequence of increasing amounts (1-, 5-, 10-, and 20-fold molar excess) of PIP_2. (H) SDS−PAGE without cross-linking to reveal homo- and heterodimerization of Vt (residues 879−1066) as a consequence of PIP_2 (145 μM). Vt dimers are seen in the presence (lane b) but not in the absence (lane a) of PIP_2. MVt dimers are seen in the presence (lane f) but not in the absence (lane g) of PIP_2. Vt/MVt heterodimers are seen in the presence of PIP_2 (lanes c−e).

mutant (Figure 1A−C) that binds to PIP_2.[1] All proteins showed increased levels of oligomer formation induced by 15% PIP_2 containing PC micelles compared to 30 μM PIP_2 but not in the absence of PIP_2 or EDC (lanes d and e vs lanes a−c and f in Figure 1B). This suggests that oligomer formation that is observed only in the presence of PIP_2 and cross-linking might be due to nonspecific Vt oligomerization, as observed after conjugation of peptides to carrier antigens, while the crystal structure and binding studies (below) argue for specificity of lipid-induced dimerization.

We confirmed the identity of our bands by immunoblotting (Figure 1D). The metavinculin tail domain MVt was reported to differ in its oligomerization ability compared to that of Vt, where trimers were observed for only Vt but never for MVt.[46] We obtained similar results for MVt (residues 879−1134) where MVt dimers formed at 20-fold molar PIP_2 excess (Figure 1E). However, our metavinculin crystal structures[50] showed that the MVt domain (originally defined as metavinculin residues 858−1134)[9] corresponding to Vt is truncated, and indeed, structurally equivalent MVt constructs comprising only the five-helix bundle (vinculin residues 879−1066 and metavinculin residues 945−1134, Figure 1F, or 959−1130, Figure 1G) did form trimers upon binding to PIP_2. Thus, the N-terminal region of MVt (metavinculin residues 858−946) inhibits PIP_2-induced trimer formation.

Finally, the fact that we obtained Vt oligomers that were resistant to SDS treatment, as seen for example for membrane proteins with strong hydrophobic interactions, prompted us to examine the oligomerization without cross-linking (Figure 1H). In the absence of PIP_2, a single band was obtained for the corresponding polypeptide chain. Surprisingly, in the presence of PIP_2, a second band corresponding to the molecular weight of the respective Vt or MVt dimer was also observed. Finally, in the presence of both Vt and MVt as well as PIP_2, the PIP_2-induced Vt/MVt heterodimer can be seen via SDS−PAGE.

Effects of Binding of PIP_2 on Merlin Oligomerization. Because our lipid-binding deficient vinculin mutants showed oligomerization properties similar to those of wild-type vinculin, we tested whether another PIP_2-binding protein that does not oligomerize can also form oligomers in the presence of PIP_2 and EDC/NHS. We chose another cytoskeletal protein, the tumor suppressor protein merlin that was shown to be monomeric in its PIP_2-bound conformation.[71] To our surprise, we found that the full-length protein and the N-terminal FERM domain harboring the PIP_2-binding site formed dimers with 30 μM PIP_2 even in the absence of EDC/NHS that were resistant to SDS treatment (Figure 2). Dimers were also observed in the absence of PIP_2 after cross-linking as we found for vinculin. Furthermore, binding of PIP_2 or a short chain (C8) PIP_2 derivative and EDC/NHS cross-linking induced dimers, trimers, and tetramers that could readily be seen via SDS−PAGE, as was also the case for vinculin, but with significant reduction of the remaining monomeric merlin species, at least in the case of the N-terminal merlin domain. Given the background dimer formation with just EDC/NHS, it was not surprising to also see dimer formation for merlin incubated with PC micelles. However, higher-order oligomers were observed only for PC micelles containing 15% PIP_2. Because PIP_2-bound merlin is monomeric in solution as determined by static light scattering and small angle neutron scattering,[71] the established cross-linking assay seems to favor oligomer interactions.

Vinculin Oligomerizes under Physiological Conditions. Because of oligomer formation resulting from cross-linking, we performed size exclusion chromatography (SEC) expecting to see individual peaks that would correspond to the distinct oligomeric states of Vt in the presence of PIP_2.

DOI: 10.1021/acs.biochem.5b00015
Biochemistry 2015, 54, 2758−2768

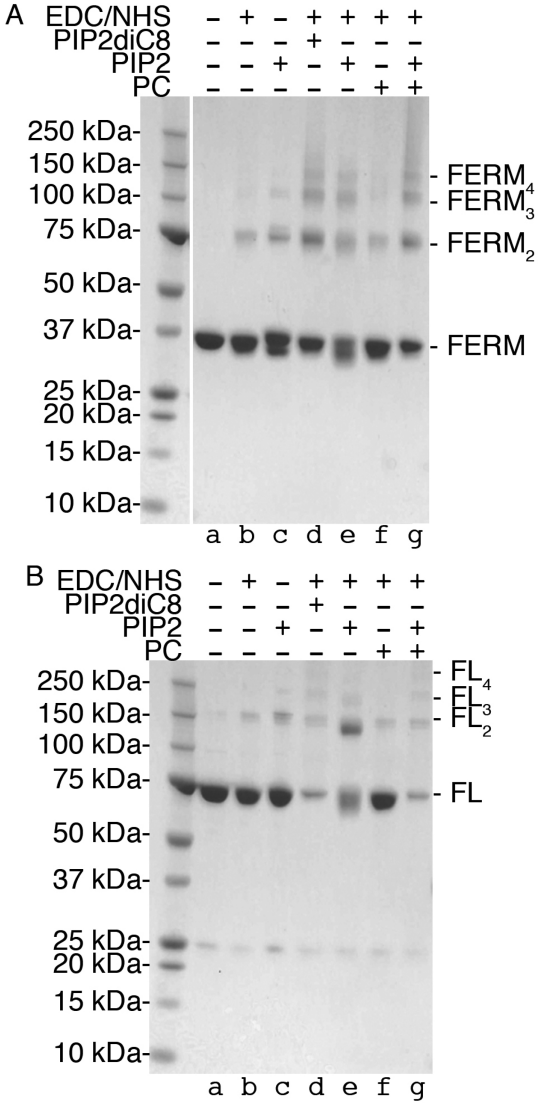

Figure 2. Binding of merlin to PIP_2 induces the formation of oligomers. SDS−PAGE of (A) the merlin N-terminal domain or (B) full-length (FL) human merlin protein after EDC/NHS cross-linking to reveal oligomerization as a consequence of diC8-PIP_2 (lane d) or PIP_2 (lane e). PIP_2-induced dimerization is also observed in the absence of EDC/NHS (lane c), while proteins alone do not oligomerize (lane a) but form dimers in the presence of EDC/HNS (lane b). Oligomerization was also observed in the presence of PC/PIP_2 micelles (lane g) but not in PC micelles alone (lane f).

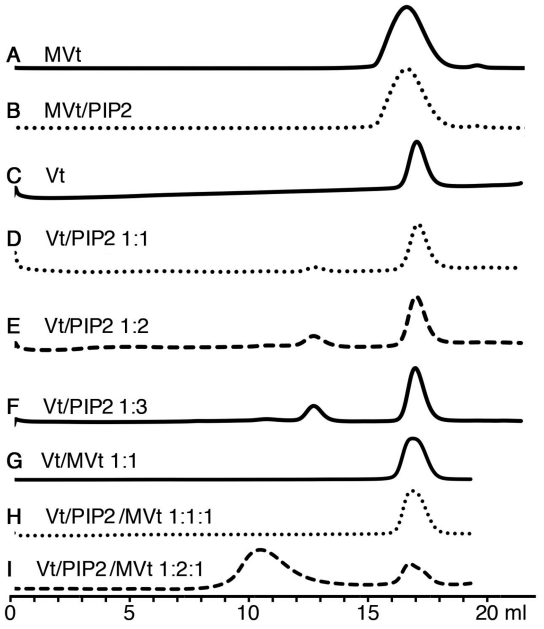

Figure 3. Vinculin and metavinculin differ in their PIP_2-induced oligomerization properties. Size exclusion chromatogram (ordinate, relative A_{280}) of the 19.8 kDa metavinculin tail domain, MVt, (A) without and (B) with PIP_2 (loaded at a MVt:PIP_2 ratio of 1:1) eluting at 16.65 mL (corresponding to an apparent molecular weight of 21.8 kDa) and 16.64 mL (corresponding to an apparent molecular weight of 21.9 kDa), respectively; the 19.74 kDa vinculin tail domain, Vt, (C) without (eluting at 17.11 mL corresponding to an apparent molecular weight of 17.9 kDa) or with (D) a 1-fold molar excess of PIP_2 (eluting at 12.81 mL corresponding to an apparent molecular weight of 117.5 kDa), (E) a 2-fold molar excess of PIP_2 (eluting at 12.76 mL corresponding to an apparent molecular weight of 120.1 kDa consistent with a hexamer), or (F) a 3-fold molar excess of PIP_2 (eluting at 12.76 mL corresponding to an apparent molecular weight of 120.1 kDa consistent with a hexamer), which is the maximum concentration to keep proteins soluble and PIP_2 below the critical micelle concentration; and the 39.54 kDa Vt/MVt complex (G) without (eluting at 16.89 mL corresponding to an apparent molecular weight of 19.7 kDa corresponding to the individual Vt or MVt polypeptide chain) or with (H) a 1-fold (eluting at 16.87 mL corresponding to an apparent molecular weight of 19.9 kDa) or (I) 2-fold molar excess of PIP_2 (eluting at 10.45 mL corresponding to an apparent molecular weight of 329.7 kDa consistent with four Vt/MVt heterodimers).

Interestingly, the muscle-specific vinculin splice variant termed metavinculin is significantly impaired in forming such dimers during the same cross-linking assay, and trimers were not observed even after immunoblotting.[46] Indeed, the metavinculin tail domain MVt eluted as a monomer in the presence or absence of PIP_2 (Figure 3A,B). However, Vt formed increasing amounts of what appears to be hexamers with increasing amounts of PIP_2 (Figure 3C−F). Finally, at a 2-fold molar excess of PIP_2 (but not 1-fold), vinculin formed an oligomer consistent with four heterodimers with metavinculin (Figure 3G−I). These results caution again about the overinterpretation of the cross-linking data.

Vt/PIP_2 Binds Vinculin and Metavinculin with Nanomolar Affinity. The discrepancies in oligomerization prompted us to characterize the binding of the Vt/PIP_2 complex to Vt or MVt by using a PIP_2 derivative having a short phosphoinositide chain [$(CH_2)_8$] that does not allow micelle formation. Using Biacore 2000 biosensor equipment with a CM5 sensor chip, we immobilized Vt and MVt on flow cells (Figure 4A,B). Vt was immobilized at approximately 6000 RU, and MVt was biotinylated and captured to immobilized streptavidin at approximately 5000 RU (Figure 4C,D). Vt/PIP_2 was diluted to 1.8 μM in running buffer and was tested for binding to (Figure 4E) Vt and MVt (Figure 4F) at concentrations of 1.8, 0.6, 0.2, 0.06, 0.022, 0.007, and 0.0025 μM. Both vinculin isoforms displayed strong dimerization with Vt/PIP_2 with binding constants of 20 and 15 nM for Vt and MVt, respectively, and binding capacities, R_{max}, of 32 and 3.1, respectively. The data are consistent with a second binding site of 1.49 and 1.37 nM for Vt/PIP_2 binding for Vt and MVt, respectively, with R_{max} values of 478 and 74.2, respectively. Data were fit using Langmuir's two-binding site model to a hyperbola. Further, this model suggests that the Vt/PIP_2

DOI: 10.1021/acs.biochem.5b00015
Biochemistry 2015, 54, 2758−2768

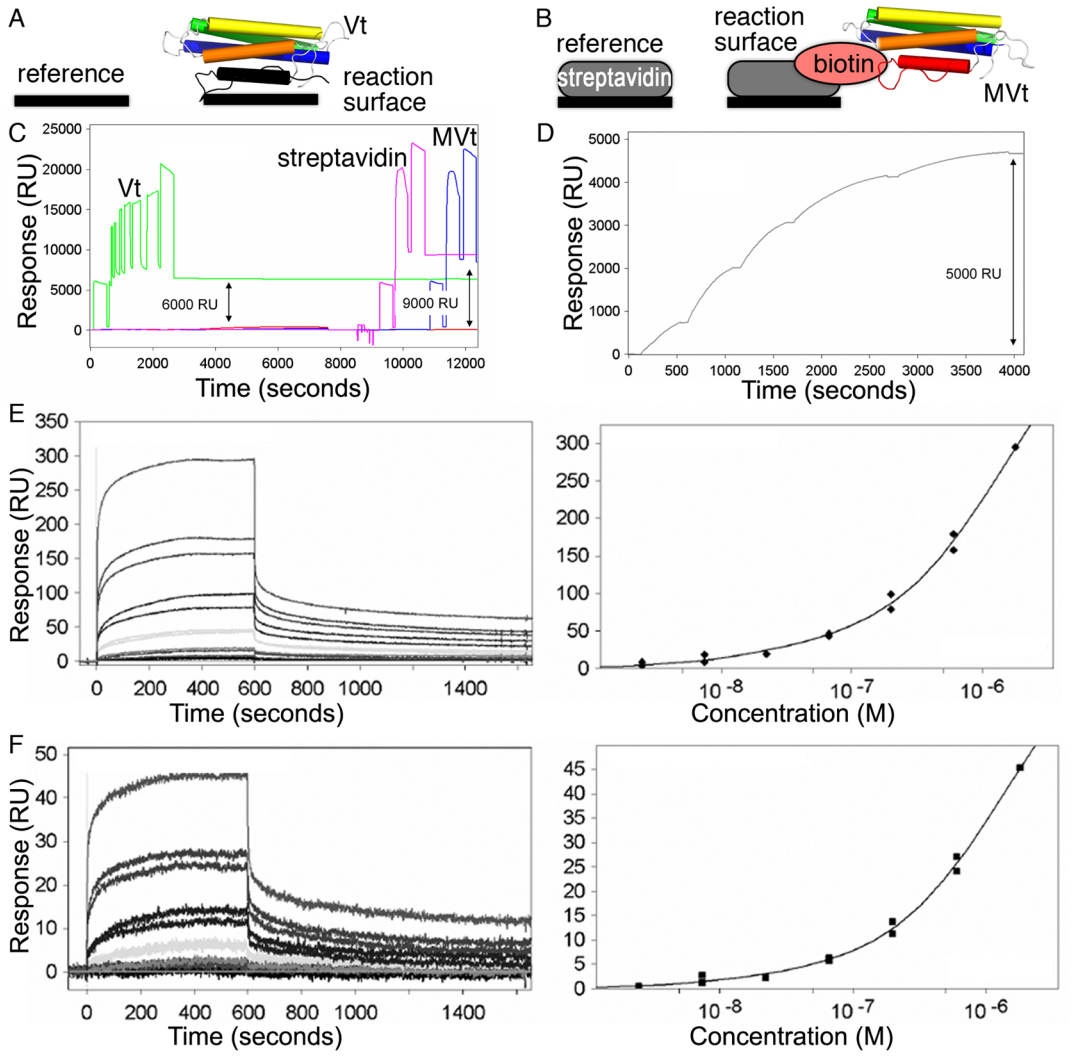

Figure 4. Vinculin and metavinculin bind PIP_2 with comparable affinities. Biacore surface plasmon resonance (SPR) was used to measure the affinity of PIP_2. Schematic of (A) Vt immobilization and (B) MVt capture. (C) SPR signal traces or responses corresponding to different fluidic channels or flow cells. Immobilization of Vt was performed using HBS-P buffer [10 mM HEPES (pH 7.4), 150 mM NaCl, and 0.005% P-20] at 25 °C using standard amine coupling chemistry. Approximately 6000 RU of Vt was immobilized on the reaction surface flow cell. Direct immobilization of MVt on the CM5 chip surface was not possible because of precipitation of MVt in sodium acetate, and therefore, MVt was biotinylated and captured to the streptavidin surface, which was built on the reference and reaction surface using standard amine coupling chemistry at a density of ~9000 RU. Vt and MVt were immobilized on flow cells 2 (green trace) and 4 (blue trace), respectively. Flow cells 1 (red trace) and 3 (magenta trace) served as a reference for the subtraction of any background signal and nonspecific binding. Different color traces represent the signals from the four different flow cells. (D) SPR signal response after injection of biotinylated MVt on streptavidin-coated chips. The capture of MVt was performed by incubation with NHS-biotin at an equimolar ratio in HBS-P buffer for 2 h. Free biotin was removed from solution using a fast desalting column. Biotinylated MVt was captured to the streptavidin surface at flow cell 4 with a significant response of approximately 5000 RU. (E and F) Representative sensograms (left panels) depicting the association and dissociation of Vt/PIP_2 to immobilized Vt (E) and MVt (F) at various concentrations (1.8, 0.6, 0.2, 0.06, 0.022, 0.007, and 0.0025 μM). The initial 600 s indicates the phase of association of Vt/PIP_2 with Vt or MVt, and the later part of the traces represents the dissociation phase. The concentration-dependent binding is observed through an increased response (RU) with an increasing concentration of the Vt/PIP_2 complex (analyte). The response units obtained are plotted as a function of concentration (right panel) to derive the affinities of the observed interaction. In the right panels, the *X*-axis represents the concentration of Vt/PIP_2 (on a logarithmic scale) and the *Y*-axis the maximal response (RU) at equilibrium. The data were fit using a two-binding site model. Vt/PIP_2 bound to the Vt and MVt surfaces with calculated affinities of 20 and 15 nM, respectively. A detailed description of the data analysis is given in the Results. Representative sensograms are shown in the left panels. The right panels plot the responses as a function of concentration (on a logarithmic scale) to calculate the affinities of the interaction.

complex binds at least two different regions on the Vt or MVt protein: a high-affinity (K_d values of 1.49 nM for Vt and 1.37 nM for MVt) binding site detected at low Vt/PIP_2 concentrations (1−2.5 nM) and a lower-affinity (K_d values of 20 nM for Vt and 15 nM for MVt) binding site observed only at higher Vt/PIP_2 concentrations (7.5−22 nM).

PIP_2 Induces Wild-Type but Not Lipid Deficient Vt Dimerization. To monitor PIP_2-induced Vt dimerization, we used CFP-Vt and YPF-Vt FRET probes as the donor−acceptor pair (Figure 5A,B). We measured the emission spectra for individual proteins independently to determine the most suitable concentrations of CFP- and YFP-labeled Vt proteins for FRET measurements. We recorded the emission spectra at

DOI: 10.1021/acs.biochem.5b00015
Biochemistry 2015, 54, 2758−2768

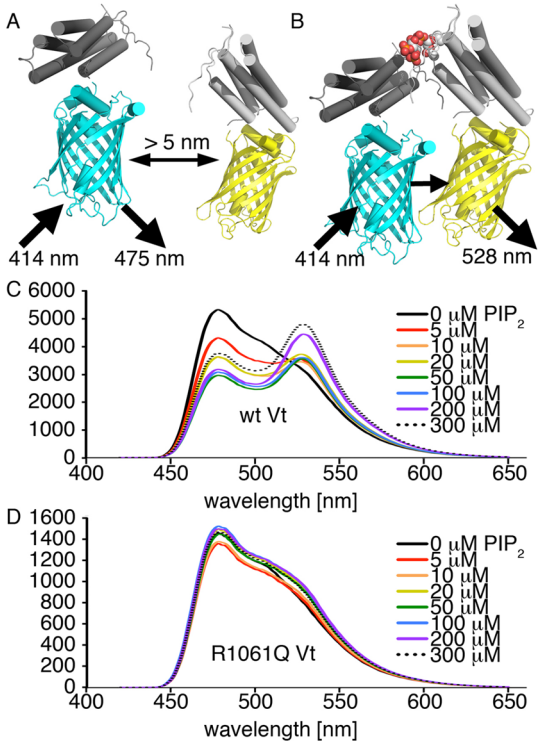

Figure 5. PIP_2 micelles induce dimerization of the wild type but not lipid-binding deficient vinculin. (A) Schematic representation of fluorescence emissions of PIP_2-bound fluorescently tagged Vt proteins, colored dark and light gray, respectively. We used the traditional CFP donor and YPF acceptor FRET pairs, colored cyan and yellow, respectively. If the two fluorescent moieties are more than 5 nm apart, excitation of the donor CFP results in only observable emission from the donor. (B) Binding of Vt to PIP_2 (shown as spheres) induces an interaction between the Vt ligand and the Vt sensor domain that brings the two fluorescent moieties within range (<5 nm) where the excitation of the donor CFP is propagated to the acceptor YFP through nonradiative photon transfer resulting in emission from the YFP acceptor. (C) Emission spectra of 1.5 μM CFP-Vt and 4 μM YFP-Vt in the absence (black) and presence of increasing concentrations of PIP_2 (5 μM, red; 10 μM, orange; 20 μM, yellow; 50 μM, green; 100 μM, blue; 200 μM, violet; and 300 μM, dotted black) upon excitation at 414 nm. Two emission peaks at 475 and 528 nm are determined in the presence of PIP_2 for Vt constructs, indicating that FRET occurred between CFP-Vt and YFP-Vt proteins. The ordinate shows the relative fluorescence. (D) Emission spectra of 1.5 μM CFP-Vt K1061Q and 4 μM YFP-Vt K1061Q mutants in the absence (black) and presence of increasing concentrations of PIP_2 (5 μM, red; 10 μM, orange; 20 μM, yellow; 50 μM, green; 100 μM, blue; 200 μM, violet; and 300 μM, dotted black) upon excitation at 414 nm. Addition of PIP_2 to the reaction mixture has showed an emission maximum at only 475 nm, not at 528 nm, indicating that no FRET occurred between fluorescently labeled mutant Vt proteins.

475 nm for different concentrations of CFP-Vt (0.1, 0.5, 1.0, and 1.5 μM) at an excitation wavelength of 414 nm using a 455 nm cutoff filter and found that 1.5 μM CFP-Vt showed the highest emission intensity without saturating the fluorescence detector. We measured the emission spectra at 528 nm for varying concentrations of YFP-Vt (1, 2, 3, and 4 μM) using an excitation wavelength of 475 nm and a cutoff filter of 495 nm and found that 4 μM YFP-Vt showed the highest emission spectra without saturation. We excited a mixture of CFP-Vt and YFP-Vt in the presence of increasing concentrations of PIP_2 at 414 nm and observed two emission peaks at 475 and 528 nm, respectively (Figure 5C). Emission at 475 nm results from emission of unquenched CFP-Vt (fluorescence donor). The emission intensity at 528 nm consists of the direct emission of unquenched CFP-Vt, the direct emission of YFP-Vt, which is minimal (for example, in the absence of PIP_2), and the emission of YFP-Vt excited by energy transferred from CFP-Vt (Figure 5B). However, in the absence of PIP_2, there is a strong emission peak at 475 nm and only some emission maxima at 528 nm observed for the minimal spectral bleed-through and/or lipid-independent interaction (Figure 5C). When the mixture of K1061Q mutant CFP-Vt and K1061Q mutant YFP-Vt in the presence and absence of PIP_2 was excited at 414 nm, single emission peaks were observed at 475 nm (Figure 5D). Emission at 475 nm results from the emission of unquenched CFP-Vt [fluorescence donor (Figure 5A)]. For the lipid-binding deficient Vt K1061Q mutant, there was no difference in the emission spectra in the absence and presence of PIP_2, indicating that PIP_2 does not interact with the mutant Vt protein consistent with lipid binding assays.[1] The minimal emission intensity at 528 nm shows the acceptor (YFP) spectral bleed-through and/or lipid-independent interaction, which is same for both mutant proteins in the presence and absence of PIP_2 (Figure 5D).

DISCUSSION

Vinculin oligomerization is important for its F-actin bundling and scaffolding functions. Vinculin was shown to form multimers, especially at high (500 mM) salt concentrations.[54,55] However, all biochemical characterizations of the vinculin oligomer relied on chemical cross-linking in the presence[46,53] or absence[53,58,59] of PIP_2. Surprisingly, we found that the lipid-binding deficient mutants (K915Q/K944Q/R945Q, K915Q/K1061Q, and K944Q/R945Q/K1061Q) behaved like wild-type Vt, and all formed dimers, trimers, tetramers, and pentamers in the presence of PIP_2 that were easily visualized via SDS−PAGE (Figure 1A−C) and immunoblotting (Figure 1D). This suggested that oligomer formation might be an artifact of cross-linking. Indeed, nonspecific interactions with PIP_2 have also been reported for the microtubule-associated protein tau with a K_d of 4.8 μM.[72]

Furthermore, while MVt has never been shown to form trimers, we obtained PIP_2-induced MVt dimers and trimers upon chemical cross-linking when using truncated MVt constructs [residues 879−1134, 945−1134, or 959−1130 (Figure 1E−G)], compared to the construct of residues 858−1134 used previously.[46] The biggest surprise came from analyzing PIP_2-adsorbed Vt or MVt via SDS−PAGE without chemical cross-linking where Vt and MVt homodimers were readily visible as well as Vt/MVt heterodimers (Figure 1H). Furthermore, there was significant depletion of monomeric Vt upon heterodimer formation. Clearly, Vt forms highly stable homo- and heterodimers in solution. Similarly, stable heterodimers have been reported for Vt and full-length metavinculin by pull-down assays.[50]

Because our lipid-binding deficient Vt mutants also oligomerized like wild-type Vt in the presence of EDC and PIP_2, we sought to develop an unbiased assay to characterize the lipid-induced oligomer. First, as a control, we examined another PIP_2-binding protein, merlin, which has been shown to remain monomeric when bound to PIP_2 and where values for binding of PIP_2 to full-length merlin and the phosphomimetic S518D mutant were 650 and 961 nM, respectively.[71] As determined by SANS and DLS, wild-type merlin adopts a more

DOI: 10.1021/acs.biochem.5b00015
Biochemistry 2015, 54, 2758−2768

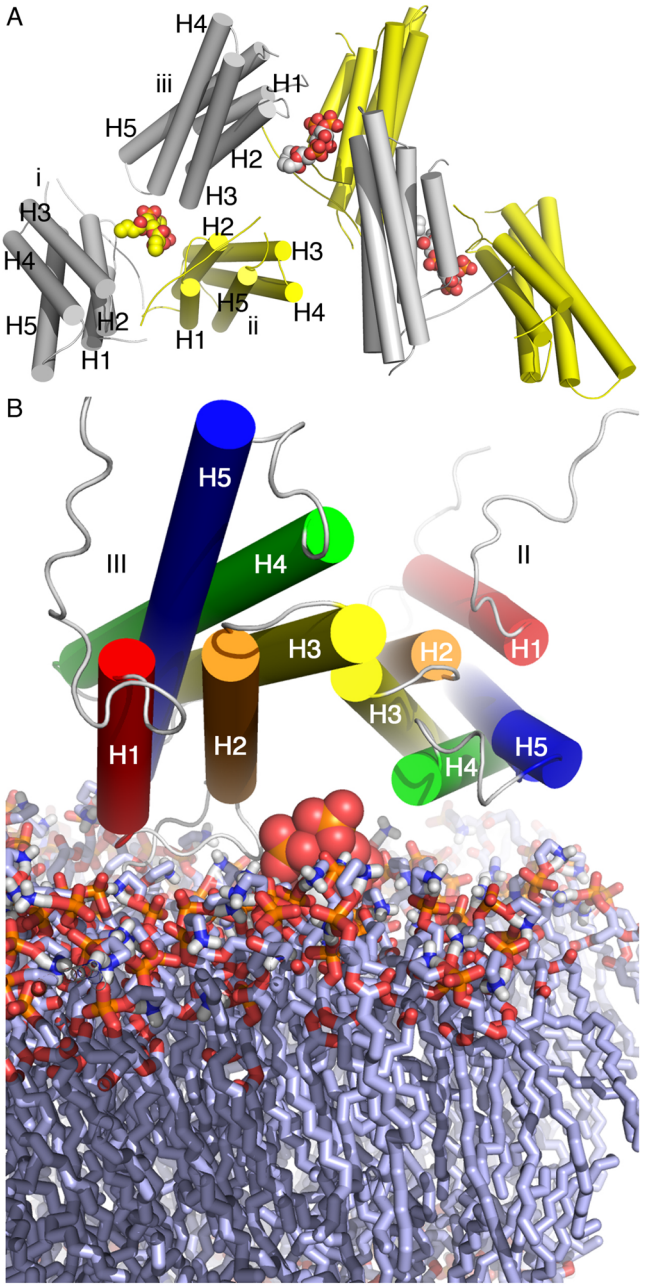

Figure 6. PIP_2-induced vinculin oligomerization. (A) In the Vt/PIP_2 crystal structure, PIP_2 bridges Vt molecule "I" (gray) with Vt molecule "II" (yellow) through interactions with the loop connecting the first two α-helices of the five-helix Vt bundle as well as the C-terminus. Vt molecule "III" from another Vt/PIP_2/Vt dimer, which corresponds to molecule "I" within this other dimer as indicated by the same gray color coding, through its interactions of its third α-helix with the PIP_2 sandwiching the first pair of Vt molecules. The three Vt/PIP_2/Vt dimers in the asymmetric unit are shown. (B) Docking of the Vt/PIP_2/Vt dimer, molecules "II" and "III", onto a membrane reveals that a dimer, not a higher-order oligomer, is compatible with binding of vinculin to the membrane. Vt α-helices are colored spectrally and labeled H1–H5. The PIP_2 in the Vt/PIP_2/Vt dimer is shown as spheres.

open conformation and is a monomer when bound to PIP_2, while the S518D merlin mutant is in a closed conformation and also monomeric when bound to PIP_2.[71] The A585W/R588K merlin mutant used in our study was determined to be the most tightly closed monomer.[73,74] Surprisingly, both the full-length domain and the merlin N-terminal domain harboring the lipid-binding site (residues 1–295)[75,76] formed dimers in the presence of either PC, PIP_2, or EDC (Figure 2). As for Vt, higher-order oligomers were seen for both merlin constructs in the presence of PIP_2 and EDC. Because the earlier study reported precipitation, to which our constructs are not susceptible, it is unclear how much PIP_2 remained in the soluble fraction.

Next, on a size exclusion chromatography (SEC) column, only a monomeric peak is found for MVt/PIP_2, a monomeric and a second peak consistent with a hexamer for Vt/PIP_2, and only one peak consistent with four Vt/PIP_2/MVt heterodimers (Figure 3). While SEC cannot accurately determine the oligomeric state of nonglobular proteins, our results clearly show that there are not several peaks that could represent the various oligomers observed in the chemical cross-linking assay, suggesting unambiguously that there is only one oligomeric species formed.

Thus, we characterized PIP_2-induced homo- and heterodimer formation by surface plasmon resonance. The two-binding site model[77] that was used for fitting the SPR data is supported by our structural data where we have shown that PIP_2 binds to the C-terminus as well as K944 and R945 on α-helix H3 indicating two binding sites of PIP_2 on the Vt molecule.[1] The observed nanomolar homo- and heterodimer formation (Figure 4) is consistent with the dimers seen via SDS–PAGE in the absence of EDC (Figure 1H). Further, in solution, Vt clearly dimerizes as we showed by FRET (Figure 5). FRET occurs only when the donor (CFP) and acceptor (YFP) are within a Forster radius of <5 nm.[78] While FRET is sensitive to both orientation and localization, the absence of FRET does not necessarily indicate a lack of Vt association through other interaction sites. However, only wild-type CFP- and YFP-tagged Vt proteins showed a FRET signal in the presence of PIP_2, indicating that PIP_2 is mediating the dimerization of Vt molecules. Moreover, our PIP_2-binding deficient mutant K1061Q[1] showed no FRET signal even at higher concentrations of PIP_2, indicating that PIP_2 binding is necessary for the vinculin tail domains to interact at focal adhesion sites. Significantly, while higher-order oligomers are seen in the crystal structure (Figure 6A), steric hindrance prevents such conformers on a flat surface such as at the plasma membrane, which is only consistent with dimer formation (Figure 6B). Collectively, our studies clearly demonstrate that PIP_2 binding induces vinculin dimer formation under physiological conditions. Our studies are of interest in understanding of how PIP_2 regulates clustering, sequestration, and activation of vinculin at the cell membrane and provide insight into the mechanism, specificity, and dimerization of vinculin in transmitting a message.

AUTHOR INFORMATION

Corresponding Author

*Cell Adhesion Laboratory, Department of Cancer Biology, The Scripps Research Institute, 130 Scripps Way, Jupiter, FL 33458. E-mail: cmorrow@scripps.edu. Telephone: (561) 228-3249. Fax: (561) 228-3068.

Funding

T.I. is supported by grants from the National Institute of General Medical Sciences from the National Institutes of Health and by start-up funds provided to Scripps Florida by the State of Florida.

DOI: 10.1021/acs.biochem.5b00015
Biochemistry 2015, 54, 2758–2768

Notes

The authors declare no competing financial interest.

■ ACKNOWLEDGMENTS

We are indebted to David Myszka (University of Utah, Salt Lake City, UT) for surface plasmon resonance expertise. This is publication 28091 from The Scripps Research Institute.

■ ABBREVIATIONS

CFP, cyan fluorescence protein; FRET, fluorescence resonance energy transfer; MVt, metavinculin tail domain; PI, phosphatidylinositol; PIP_2, phosphatidylinositol 4,5-bisphosphate; PS, phosphatidylserine; SDS−PAGE, sodium dodecyl sulfate−polyacrylamide gel electrophoresis; SEC, size exclusion chromatography; SPR, surface plasmon resonance; VH, vinculin head domain; Vt, vinculin tail domain; YFP, yellow fluorescence protein.

■ REFERENCES

(1) Chinthalapudi, K., Rangarajan, E. S., Patil, D. N., George, E. M., Brown, D. T., and Izard, T. (2014) Lipid binding promotes oligomerization and focal adhesion activity of vinculin. *J. Cell Biol. 207*, 643−656.

(2) Parsons, J. T., Horwitz, A. R., and Schwartz, M. A. (2010) Cell adhesion: Integrating cytoskeletal dynamics and cellular tension. *Nat. Rev. Mol. Cell Biol. 11*, 633−643.

(3) Ziegler, W. H., Liddington, R. C., and Critchley, D. R. (2006) The structure and regulation of vinculin. *Trends Cell Biol. 16*, 453−460.

(4) Xu, W., Baribault, H., and Adamson, E. D. (1998) Vinculin knockout results in heart and brain defects during embryonic development. *Development 125*, 327−337.

(5) Xu, W., Coll, J. L., and Adamson, E. D. (1998) Rescue of the mutant phenotype by reexpression of full-length vinculin in null F9 cells; effects on cell locomotion by domain deleted vinculin. *J. Cell Sci. 111*, 1535−1544.

(6) Zemljic-Harpf, A. E., Ponrartana, S., Avalos, R. T., Jordan, M. C., Roos, K. P., Dalton, N. D., Phan, V. Q., Adamson, E. D., and Ross, R. S. (2004) Heterozygous inactivation of the vinculin gene predisposes to stress-induced cardiomyopathy. *Am. J. Pathol. 165*, 1033−1044.

(7) Byrne, B. J., Kaczorowski, Y. J., Coutu, M. D., and Craig, S. W. (1992) Chicken vinculin and meta-vinculin are derived from a single gene by alternative splicing of a 207-base pair exon unique to meta-vinculin. *J. Biol. Chem. 267*, 12845−12850.

(8) Maeda, M., Holder, E., Lowes, B., Valent, S., and Bies, R. D. (1997) Dilated cardiomyopathy associated with deficiency of the cytoskeletal protein metavinculin. *Circulation 95*, 17−20.

(9) Olson, T. M., Illenberger, S., Kishimoto, N. Y., Huttelmaier, S., Keating, M. T., and Jockusch, B. M. (2002) Metavinculin mutations alter actin interaction in dilated cardiomyopathy. *Circulation 105*, 431−437.

(10) Coll, J. L., Ben-Ze'ev, A., Ezzell, R. M., Rodriguez Fernandez, J. L., Baribault, H., Oshima, R. G., and Adamson, E. D. (1995) Targeted disruption of vinculin genes in F9 and embryonic stem cells changes cell morphology, adhesion, and locomotion. *Proc. Natl. Acad. Sci. U.S.A. 92*, 9161−9165.

(11) Subauste, M. C., Pertz, O., Adamson, E. D., Turner, C. E., Junger, S., and Hahn, K. M. (2004) Vinculin modulation of paxillin-FAK interactions regulates ERK to control survival and motility. *J. Cell Biol. 165*, 371−381.

(12) Borgon, R. A., Vonrhein, C., Bricogne, G., Bois, P. R., and Izard, T. (2004) Crystal structure of human vinculin. *Structure 12*, 1189−1197.

(13) Izard, T., Evans, G., Borgon, R. A., Rush, C. L., Bricogne, G., and Bois, P. R. (2004) Vinculin activation by talin through helical bundle conversion. *Nature 427*, 171−175.

(14) Bakolitsa, C., de Pereda, J. M., Bagshaw, C. R., Critchley, D. R., and Liddington, R. C. (1999) Crystal structure of the vinculin tail suggests a pathway for activation. *Cell 99*, 603−613.

(15) Winkler, J., Lunsdorf, H., and Jockusch, B. M. (1996) The ultrastructure of chicken gizzard vinculin as visualized by high-resolution electron microscopy. *J. Struct. Biol. 116*, 270−277.

(16) Burridge, K., and Mangeat, P. (1984) An interaction between vinculin and talin. *Nature 308*, 744−746.

(17) Izard, T., and Vonrhein, C. (2004) Structural basis for amplifying vinculin activation by talin. *J. Biol. Chem. 279*, 27667−27678.

(18) Yogesha, S. D., Rangarajan, E. S., Vonrhein, C., Bricogne, G., and Izard, T. (2012) Crystal structure of vinculin in complex with vinculin binding site 50 (VBS50), the integrin binding site 2 (IBS2) of talin. *Protein Sci. 21*, 583−588.

(19) Yogesha, S. D., Sharff, A., Bricogne, G., and Izard, T. (2011) Intermolecular versus intramolecular interactions of the vinculin binding site 33 of talin. *Protein Sci. 20*, 1471−1476.

(20) Wachsstock, D. H., Wilkins, J. A., and Lin, S. (1987) Specific interaction of vinculin with α-actinin. *Biochem. Biophys. Res. Commun. 146*, 554−560.

(21) Bois, P. R., O'Hara, B. P., Nietlispach, D., Kirkpatrick, J., and Izard, T. (2006) The vinculin binding sites of talin and α-actinin are sufficient to activate vinculin. *J. Biol. Chem. 281*, 7228−7236.

(22) Watabe-Uchida, M., Uchida, N., Imamura, Y., Nagafuchi, A., Fujimoto, K., Uemura, T., Vermeulen, S., van Roy, F., Adamson, E. D., and Takeichi, M. (1998) α-Catenin-vinculin interaction functions to organize the apical junctional complex in epithelial cells. *J. Cell Biol. 142*, 847−857.

(23) Weiss, E. E., Kroemker, M., Rudiger, A. H., Jockusch, B. M., and Rudiger, M. (1998) Vinculin is part of the cadherin-catenin junctional complex: Complex formation between α-catenin and vinculin. *J. Cell Biol. 141*, 755−764.

(24) Rangarajan, E. S., and Izard, T. (2012) α-Catenin unfurls upon binding to vinculin. *J. Biol. Chem. 287*, 18492−18499.

(25) Rangarajan, E. S., and Izard, T. (2013) Dimer asymmetry defines α-catenin interactions. *Nat. Struct. Mol. Biol. 20*, 188−193.

(26) Peng, X., Cuff, L. E., Lawton, C. D., and DeMali, K. A. (2010) Vinculin regulates cell-surface E-cadherin expression by binding to β-catenin. *J. Cell Sci. 123*, 567−577.

(27) Hazan, R. B., Kang, L., Roe, S., Borgen, P. I., and Rimm, D. L. (1997) Vinculin is associated with the E-cadherin adhesion complex. *J. Biol. Chem. 272*, 32448−32453.

(28) Reinhard, M., Rudiger, M., Jockusch, B. M., and Walter, U. (1996) VASP interaction with vinculin: A recurring theme of interactions with proline-rich motifs. *FEBS Lett. 399*, 103−107.

(29) Mandai, K., Nakanishi, H., Satoh, A., Takahashi, K., Satoh, K., Nishioka, H., Mizoguchi, A., and Takai, Y. (1999) Ponsin/SH3P12: An l-afadin- and vinculin-binding protein localized at cell-cell and cell-matrix adherens junctions. *J. Cell Biol. 144*, 1001−1017.

(30) Kioka, N., Sakata, S., Kawauchi, T., Amachi, T., Akiyama, S. K., Okazaki, K., Yaen, C., Yamada, K. M., and Aota, S. (1999) Vinexin: A novel vinculin-binding protein with multiple SH3 domains enhances actin cytoskeletal organization. *J. Cell Biol. 144*, 59−69.

(31) DeMali, K. A., Barlow, C. A., and Burridge, K. (2002) Recruitment of the Arp2/3 complex to vinculin: Coupling membrane protrusion to matrix adhesion. *J. Cell Biol. 159*, 881−891.

(32) Wood, C. K., Turner, C. E., Jackson, P., and Critchley, D. R. (1994) Characterisation of the paxillin-binding site and the C-terminal focal adhesion targeting sequence in vinculin. *J. Cell Sci. 107*, 709−717.

(33) Huttelmaier, S., Illenberger, S., Grosheva, I., Rudiger, M., Singer, R. H., and Jockusch, B. M. (2001) Raver1, a dual compartment protein, is a ligand for PTB/hnRNPI and microfilament attachment proteins. *J. Cell Biol. 155*, 775−786.

(34) Lee, J. H., Rangarajan, E. S., Vonrhein, C., Bricogne, G., and Izard, T. (2012) The metavinculin tail domain directs constitutive interactions with raver1 and vinculin RNA. *J. Mol. Biol. 422*, 697−704.

DOI: 10.1021/acs.biochem.5b00015
Biochemistry 2015, 54, 2758−2768

(35) Lee, J. H., Rangarajan, E. S., Yogesha, S. D., and Izard, T. (2009) Raver1 interactions with vinculin and RNA suggest a feed-forward pathway in directing mRNA to focal adhesions. *Structure 17*, 833−842.
(36) Rangarajan, E. S., Lee, J. H., and Izard, T. (2011) Apo raver1 structure reveals distinct RRM domain orientations. *Protein Sci. 20*, 1464−1470.
(37) Huttelmaier, S., Bubeck, P., Rudiger, M., and Jockusch, B. M. (1997) Characterization of two F-actin-binding and oligomerization sites in the cell-contact protein vinculin. *Eur. J. Biochem. 247*, 1136−1142.
(38) Johnson, R. P., Niggli, V., Durrer, P., and Craig, S. W. (1998) A conserved motif in the tail domain of vinculin mediates association with and insertion into acidic phospholipid bilayers. *Biochemistry (Moscow) 37*, 10211−10222.
(39) Ito, S., Werth, D. K., Richert, N. D., and Pastan, I. (1983) Vinculin phosphorylation by the src kinase. Interaction of vinculin with phospholipid vesicles. *J. Biol. Chem. 258*, 14626−14631.
(40) Johnson, R. P., and Craig, S. W. (1995) The carboxy-terminal tail domain of vinculin contains a cryptic binding site for acidic phospholipids. *Biochem. Biophys. Res. Commun. 210*, 159−164.
(41) Gilmore, A. P., and Burridge, K. (1996) Regulation of vinculin binding to talin and actin by phosphatidyl-inositol-4,5-bisphosphate. *Nature 381*, 531−535.
(42) Palmer, S. M., Playford, M. P., Craig, S. W., Schaller, M. D., and Campbell, S. L. (2009) Lipid binding to the tail domain of vinculin: Specificity and the role of the N and C termini. *J. Biol. Chem. 284*, 7223−7231.
(43) Belkin, A. M., Ornatsky, O. I., Kabakov, A. E., Glukhova, M. A., and Koteliansky, V. E. (1988) Diversity of vinculin/meta-vinculin in human tissues and cultivated cells. Expression of muscle specific variants of vinculin in human aorta smooth muscle cells. *J. Biol. Chem. 263*, 6631−6635.
(44) Belkin, A. M., Ornatsky, O. I., Glukhova, M. A., and Koteliansky, V. E. (1988) Immunolocalization of meta-vinculin in human smooth and cardiac muscles. *J. Cell Biol. 107*, 545−553.
(45) Koteliansky, V. E., Ogryzko, E. P., Zhidkova, N. I., Weller, P. A., Critchley, D. R., Vancompernolle, K., Vandekerckhove, J., Strasser, P., Way, M., Gimona, M., and Small, J. V. (1992) An additional exon in the human vinculin gene specifically encodes meta-vinculin-specific difference peptide. Cross-species comparison reveals variable and conserved motifs in the meta-vinculin insert. *Eur. J. Biochem. 204*, 767−772.
(46) Witt, S., Zieseniss, A., Fock, U., Jockusch, B. M., and Illenberger, S. (2004) Comparative biochemical analysis suggests that vinculin and metavinculin cooperate in muscular adhesion sites. *J. Biol. Chem. 279*, 31533−31543.
(47) Rudiger, M., Korneeva, N., Schwienbacher, C., Weiss, E. E., and Jockusch, B. M. (1998) Differential actin organization by vinculin isoforms: Implications for cell type-specific microfilament anchorage. *FEBS Lett. 431*, 49−54.
(48) Saga, S., Hamaguchi, M., Hoshino, M., and Kojima, K. (1985) Expression of meta-vinculin associated with differentiation of chicken embryonal muscle cells. *Exp. Cell Res. 156*, 45−56.
(49) Feramisco, J. R., Smart, J. E., Burridge, K., Helfman, D. M., and Thomas, G. P. (1982) Co-existence of vinculin and a vinculin-like protein of higher molecular weight in smooth muscle. *J. Biol. Chem. 257*, 11024−11031.
(50) Rangarajan, E. S., Lee, J. H., Yogesha, S. D., and Izard, T. (2010) A helix replacement mechanism directs metavinculin functions. *PLoS One 5*, e10679.
(51) Palmer, S. M., Schaller, M. D., and Campbell, S. L. (2008) Vinculin tail conformation and self-association is independent of pH and H906 protonation. *Biochemistry (Moscow) 47*, 12467−12475.
(52) Janssen, M. E., Kim, E., Liu, H., Fujimoto, L. M., Bobkov, A., Volkmann, N., and Hanein, D. (2006) Three-dimensional structure of vinculin bound to actin filaments. *Mol. Cell 21*, 271−281.
(53) Huttelmaier, S., Mayboroda, O., Harbeck, B., Jarchau, T., Jockusch, B. M., and Rudiger, M. (1998) The interaction of the cell-contact proteins VASP and vinculin is regulated by phosphatidylinositol-4,5-bisphosphate. *Curr. Biol. 8*, 479−488.
(54) Molony, L., and Burridge, K. (1985) Molecular shape and self-association of vinculin and metavinculin. *J. Cell. Biochem. 29*, 31−36.
(55) Milam, L. M. (1985) Electron microscopy of rotary shadowed vinculin and vinculin complexes. *J. Mol. Biol. 184*, 543−545.
(56) Menkel, A. R., Kroemker, M., Bubeck, P., Ronsiek, M., Nikolai, G., and Jockusch, B. M. (1994) Characterization of an F-actin-binding domain in the cytoskeletal protein vinculin. *J. Cell Biol. 126*, 1231−1240.
(57) Abe, C., Dietrich, F., Gajula, P., Benz, M., Vogel, K. P., van Gastel, M., Illenberger, S., Ziegler, W. H., and Steinhoff, H. J. (2011) Monomeric and dimeric conformation of the vinculin tail five-helix bundle in solution studied by EPR spectroscopy. *Biophys. J. 101*, 1772−1780.
(58) Shen, K., Tolbert, C. E., Guilluy, C., Swaminathan, V. S., Berginski, M. E., Burridge, K., Superfine, R., and Campbell, S. L. (2011) The vinculin C-terminal hairpin mediates F-actin bundle formation, focal adhesion, and cell mechanical properties. *J. Biol. Chem. 286*, 45103−45115.
(59) Johnson, R. P., and Craig, S. W. (2000) Actin activates a cryptic dimerization potential of the vinculin tail domain. *J. Biol. Chem. 275*, 95−105.
(60) Thompson, P. M., Tolbert, C. E., and Campbell, S. L. (2013) Vinculin and metavinculin: Oligomerization and interactions with F-actin. *FEBS Lett. 587*, 1220−1229.
(61) Perez-Moreno, M., Avila, A., Islas, S., Sanchez, S., and Gonzalez-Mariscal, L. (1998) Vinculin but not α-actinin is a target of PKC phosphorylation during junctional assembly induced by calcium. *J. Cell Sci. 111*, 3563−3571.
(62) Steimle, P. A., Hoffert, J. D., Adey, N. B., and Craig, S. W. (1999) Polyphosphoinositides inhibit the interaction of vinculin with actin filaments. *J. Biol. Chem. 274*, 18414−18420.
(63) Tall, E. G., Spector, I., Pentyala, S. N., Bitter, I., and Rebecchi, M. J. (2000) Dynamics of phosphatidylinositol 4,5-bisphosphate in actin-rich structures. *Curr. Biol. 10*, 743−746.
(64) Saunders, R. M., Holt, M. R., Jennings, L., Sutton, D. H., Barsukov, I. L., Bobkov, A., Liddington, R. C., Adamson, E. A., Dunn, G. A., and Critchley, D. R. (2006) Role of vinculin in regulating focal adhesion turnover. *Eur. J. Cell Biol. 85*, 487−500.
(65) Peng, X., Nelson, E. S., Maiers, J. L., and DeMali, K. A. (2011) New insights into vinculin function and regulation. *Int. Rev. Cell Mol. Biol. 287*, 191−231.
(66) Wirth, V. F., List, F., Diez, G., and Goldmann, W. H. (2010) Vinculin's C-terminal region facilitates phospholipid membrane insertion. *Biochem. Biophys. Res. Commun. 398*, 433−437.
(67) Diez, G., Kollmannsberger, P., Mierke, C. T., Koch, T. M., Vali, H., Fabry, B., and Goldmann, W. H. (2009) Anchorage of vinculin to lipid membranes influences cell mechanical properties. *Biophys. J. 97*, 3105−3112.
(68) Diez, G., List, F., Smith, J., Ziegler, W. H., and Goldmann, W. H. (2008) Direct evidence of vinculin tail-lipid membrane interaction in β-sheet conformation. *Biochem. Biophys. Res. Commun. 373*, 69−73.
(69) Studier, F. W. (2005) Protein production by auto-induction in high density shaking cultures. *Protein Expression Purif. 41*, 207−234.
(70) Weekes, J., Barry, S. T., and Critchley, D. R. (1996) Acidic phospholipids inhibit the intramolecular association between the N- and C-terminal regions of vinculin, exposing actin-binding and protein kinase C phosphorylation sites. *Biochem. J. 314*, 827−832.
(71) Ali Khajeh, J., Ju, J. H., Atchiba, M., Allaire, M., Stanley, C., Heller, W. T., Callaway, D. J., and Bu, Z. (2014) Molecular Conformation of the Full-Length Tumor Suppressor NF2/Merlin: A Small-Angle Neutron Scattering Study. *J. Mol. Biol. 426*, 2755−2768.
(72) Flanagan, L. A., Cunningham, C. C., Chen, J., Prestwich, G. D., Kosik, K. S., and Janmey, P. A. (1997) The structure of divalent cation-induced aggregates of PIP2 and their alteration by gelsolin and tau. *Biophys. J. 73*, 1440−1447.
(73) Sher, I., Hanemann, C. O., Karplus, P. A., and Bretscher, A. (2012) The tumor suppressor merlin controls growth in its open state,

DOI: 10.1021/acs.biochem.5b00015
Biochemistry 2015, 54, 2758−2768

and phosphorylation converts it to a less-active more-closed state. *Dev. Cell 22*, 703−705.
(74) Hennigan, R. F., Foster, L. A., Chaiken, M. F., Mani, T., Gomes, M. M., Herr, A. B., and Ip, W. (2010) Fluorescence resonance energy transfer analysis of merlin conformational changes. *Mol. Cell. Biol. 30*, 54−67.
(75) Mani, T., Hennigan, R. F., Foster, L. A., Conrady, D. G., Herr, A. B., and Ip, W. (2011) FERM domain phosphoinositide binding targets merlin to the membrane and is essential for its growth-suppressive function. *Mol. Cell. Biol. 31*, 1983−1996.
(76) Stickney, J. T., Bacon, W. C., Rojas, M., Ratner, N., and Ip, W. (2004) Activation of the tumor suppressor merlin modulates its interaction with lipid rafts. *Cancer Res. 64*, 2717−2724.
(77) Nilsson, E. C., Storm, R. J., Bauer, J., Johansson, S. M., Lookene, A., Angstrom, J., Hedenstrom, M., Eriksson, T. L., Frangsmyr, L., Rinaldi, S., Willison, H. J., Pedrosa Domellof, F., Stehle, T., and Arnberg, N. (2011) The GD1a glycan is a cellular receptor for adenoviruses causing epidemic keratoconjunctivitis. *Nat. Med. 17*, 105−109.
(78) Clegg, R. M. (1992) Fluorescence resonance energy transfer and nucleic acids. *Methods Enzymol. 211*, 353−388.

DOI: 10.1021/acs.biochem.5b00015
Biochemistry 2015, 54, 2758−2768